$\mathcal{PT}$-Symmetric Topological Edge-Gain Effect

Alex Y. Song[,1] Xiao-Qi Sun,[2] Avik Dutt[,1] Momchil Minkov,[1] Casey Wojcik[,1] Haiwen Wang,[3]
Ian A. D. Williamson[,1] Meir Orenstein,[4] and Shanhui Fan[1,*]

[1]*Department of Electrical Engineering, Stanford University, Stanford, California 94305, USA*
[2]*Department of Physics, Stanford University, Stanford, California 94305, USA*
[3]*Department of Applied Physics, Stanford University, Stanford, California 94305, USA*
[4]*Department of Electrical Engineering, Technion—Israel Institute of Technology, Technion City, Haifa 3200003, Israel*

We demonstrate a non-Hermitian topological effect that is characterized by having complex eigenvalues only in the edge states of a topological material, despite the fact that the material is completely uniform. Such an effect can be constructed in any topological structure formed by two gapped subsystems, e.g., a quantum spin-Hall system, with a suitable non-Hermitian coupling between the spins. The resulting complex-eigenvalued edge state is robust against defects due to the topological protection. In photonics, such an effect can be used for the implementation of topological lasers, in which a uniform pumping provides gain only in the edge lasing state. Furthermore, such a topological lasing model is reciprocal and is thus compatible with standard photonic platforms.

The hallmark of an electric topological insulator is the striking contrast between its edge and its bulk characteristics [1–3]. There, the bulk is in a gapped insulating phase with a band structure having a nontrivial topology. As a result of such a nontrivial topology, the system supports gap-spanning edge states that carry charge or spin currents, and hence the edge is metallic [4–10]. Similar contrast exists for many photonic topological systems as well [11–29].

Most of the initial works on topological electronic or photonic systems assume a Hermitian Hamiltonian. On the other hand, there has been significant recent interest in exploring the topological edge states of non-Hermitian systems where gain and/or loss are present, due to their potential applications in wave control, information processing, and robust lasing [30–56]. For these applications, it would be important to be able to independently control the modal gain on the edge, so that the bulk does not interfere with the edge's functionality. In this Letter, we report such a non-Hermitian contrast between the bulk and edge: under a uniform pumping throughout the structure, the bulk shows entirely real eigenspectra, while only the edge shows gain and loss as guaranteed by the topology of the bulk. We refer to such a contrast as the *topological edge-gain effect*. Here, the bulk is in the parity-time ($\mathcal{PT}$)-exact phase protected by a topological gap, while the gapless edge states exhibit gain through a thresholdless $\mathcal{PT}$ phase transition [57–69]. We show that such an effect can be realized in any topological systems that consist of two gapped subsystems, regardless of the specific design, lattice, or any additional symmetry. As an example application, such a scheme points to a new route towards topological lasers [12,49,50,52,70–79], since

our approach is explicitly reciprocal, in contrast to existing theoretical models underlying recent experimental developments. It demonstrates that topological lasing is intrinsically compatible with reciprocity and hence with standard integrated photonic platforms. Furthermore, since modal gain only occurs at the edge under uniform pumping, the selective pumping required in previous works is relieved in our scheme.

It should be emphasized that this work is demonstrating the edge-gain effect for high dimensional systems and the physics differs from the edge-gain effect in a 1D structure [56,78,80,81]. In the latter, the edge is essentially one point and is not associated with any edge transport or robustness to edge truncation. In contrast, the edge-gain effect in higher dimensions encloses richer physics related to transport and $\mathcal{PT}$ symmetry, such as robustness to edge defects, superluminal and zero-group velocities, exceptional points, etc. These features are important for many applications such as robust lasers [11–14]. Moreover, the scheme to realize the 1D edge gain does not apply to higher dimensions either [38,56]. Our result here is conceptually novel and is of interest in a broader range of applications.

Model.—To illustrate the basic idea, we consider a concrete model as illustrated by the following Hamiltonian:

$$H = t\sum_{\langle ij \rangle} c_i^\dagger c_j + i\lambda_{\text{so}}\sum_{\langle\langle ij \rangle\rangle} v_{ij} c_i^\dagger s^z c_j + i\gamma \sum_i \rho_i c_i^\dagger s^x c_i. \quad (1)$$

This Hamiltonian describes interacting spins on a honeycomb lattice, as is depicted in Fig. 1(a). It is based on the Kane-Mele quantum spin-Hall (QSH) model [4,5]. The first
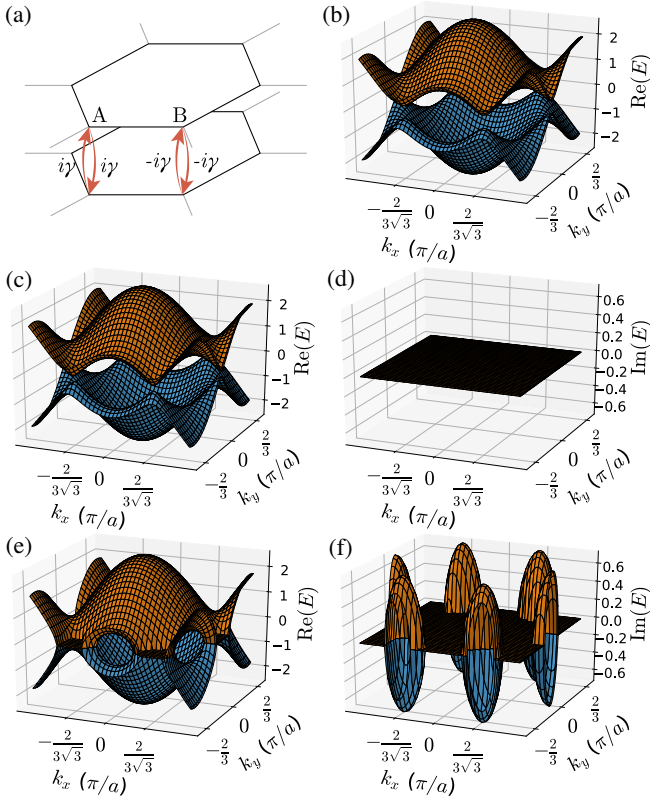
FIG. 1. (a) A schematic of the non-Hermitian QSH model. For convenience, we draw the lattices of the two spins in two layers. The added non-Hermitian couplings are indicated by the red arrows. The calculated real [(b), (c), and (e)] and imaginary [(d) and (f)] parts of the bulk band structures are shown. Here the nearest and next nearest neighbor coupling strengths are set to $t = 1$ and $\lambda_{so} = 0.05$, respectively. $\gamma = 0$ for (b), $\gamma = 0.9 \times 3\sqrt{3}\lambda_{so}$ for (c) and (d), and $\gamma = 3.0 \times 3\sqrt{3}\lambda_{so}$ for (e) and (f).

and the second terms in Eq. (1) are the nearest and second nearest neighbor couplings in the Kane-Mele model, where t and λ_{so} are the respective coupling strengths. $c_i = (c_{i\uparrow}, c_{i,\downarrow})$ is the annihilation operator for the two spins on site i. $v_{ij} = \pm 1$, depending on the orientation of the two nearest neighbor bonds going from i to j. The Pauli matrices s^i operate on the spin subspace. The third term in Eq. (1), which is added in our model, describes a non-Hermitian coupling between the spins [39]. Here γ is the coupling strength, $\rho_i = \pm 1$, depending on the sublattice index. The non-Hermitian coupling is introduced on each site uniformly.

In the momentum space, the Hamiltonian in Eq. (1) is block diagonalized as

$$h = d_1\Gamma^1 + d_{12}\Gamma^{12} + d_{15}\Gamma^{15} + i\gamma\Gamma^{13} = \begin{pmatrix} h_\uparrow & i\gamma\sigma^z \\ i\gamma\sigma^z & h_\downarrow \end{pmatrix},$$

(2)

where the first three terms form the original Kane-Mele Hamiltonian, i.e., $h_{KM} = d_1\Gamma^1 + d_{12}\Gamma^{12} + d_{15}\Gamma^{15}$. They generate the diagonal blocks in Eq. (2), where $h_{\uparrow,\downarrow}$ are the uncoupled Haldane Hamiltonians for each spin. We use the same representation for the Dirac Γ matrices as in Ref. [5], which is reproduced here: $\Gamma^{(1,2,3,4,5)} = (\sigma^x \otimes I, \sigma^z \otimes I, \sigma^y \otimes s^x, \sigma^y \otimes s^y, \sigma^y \otimes s^z)$, and the commutators are defined as $\Gamma^{ab} = [\Gamma^a, \Gamma^b]/(2i)$. Here σ^i operates in the sublattice space. It follows that $\Gamma^{12} = -\sigma^y \otimes I$, $\Gamma^{15} = \sigma^z \otimes s^z$, and $\Gamma^{13} = \sigma^z \otimes s^x$. The expressions for the coefficients are $d_1 = t(1 + 2\cos k_x /2\cos\sqrt{3}k_y/2)$, $d_{12} = -2t\cos k_x/2\sin\sqrt{3}k_y/2$, $d_{15} = \lambda_{so}(2\sin k_x - 4\sin k_x/2\cos\sqrt{3}k_y/2)$, where we have set the nearest neighbor distance to 1 [5]. The fourth term in Eq. (2) is the non-Hermitian addition to the Kane-Mele Hamiltonian. It corresponds to the off-diagonal blocks in the matrix of Eq. (2).

To understand the effect of the non-Hermitian couplings, we first note that with a zero coupling strength γ, our model reduces to that of the Kane-Mele. There, the two spins are decoupled, and the eigen spectrum is doubly degenerate with a bulk topological gap, as is shown in Fig. 1(b). The added term residing on the off-diagonal blocks in the matrix of Eq. (2) couples the two spins. However, it can be shown that such a non-Hermitian coupling does not couple the two degenerate bulk states on the same side of the gap [82]. Instead, it only couples two states of different spins on the opposite sides of the gap. After we switch on the non-Hermitian coupling, the system preserves a $\mathcal{PT}$ symmetry, where $\mathcal{P} = \sigma_x \otimes I$ is the spatial inversion, and $\mathcal{T} = I \otimes s_x K_0$ is the Bosonic time reversal operator with K_0 being the complex conjugation. To see the implication of this, in Figs. 1(c)–1(f) we plot the energy bands after we switch on the non-Hermitian coupling. With a small coupling strength of $\gamma < 3\sqrt{3}\lambda_{so}$, the bulk gap remains, and the entire system is in the $\mathcal{PT}$-exact phase, where the eigenenergies of all the bulk bands are real. With increased coupling strength γ, the energies of the modes at the upper and lower gap edge approach each other. With a larger coupling of $\gamma > 3\sqrt{3}\lambda_{so}$, the bulk gap closes as the eigenenergies of the upper and lower bands become complex conjugate pairs in the vicinity of K and K' points enclosed by exceptional rings. The system bulk thus undergoes a $\mathcal{PT}$ phase transition, where the eigenstates exhibit gain and loss.

The situation at the edge is qualitatively different from that of the bulk. In Fig. 2 we show the calculated band structure of this model in a semi-infinite stripe geometry with the zigzag boundary. Before the non-Hermitian couplings are applied, the eigen spectrum reduces to that of the original Kane-Mele model featuring a pair of gapless edge states, as is shown in Fig. 2(a). For a non-Hermitian coupling of $\gamma < 3\sqrt{3}\lambda_{so}$, the bulk bands are in the $\mathcal{PT}$-exact phase without gain or loss due to the nonzero bulk gap, as discussed above. However, the gapless edge states
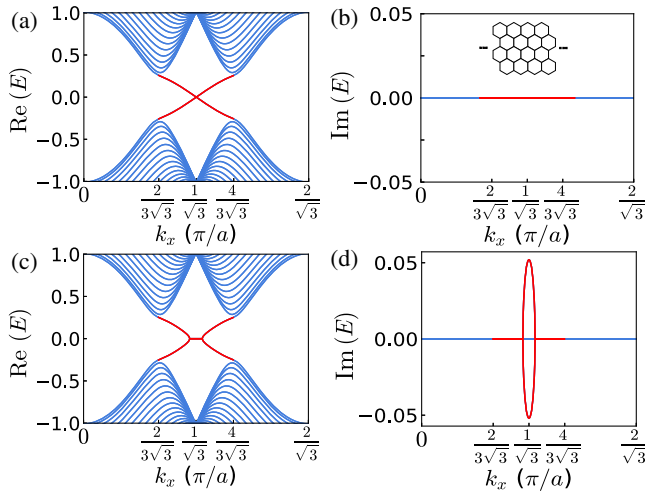
FIG. 2. Calculated real [(a) and (c)] and imaginary [(b) and (d)] part of the bands in a stripe with zigzag boundary. A schematic of the shape is shown in the inset of (b), with 30 hexagonal cells in the finite direction. $\gamma = 0$ for (a) and (b), and $\gamma = 0.2 \times 3\sqrt{3}\lambda_{so}$ for (c) and (d). The edge bands are colored in red while those of the bulk are in blue.
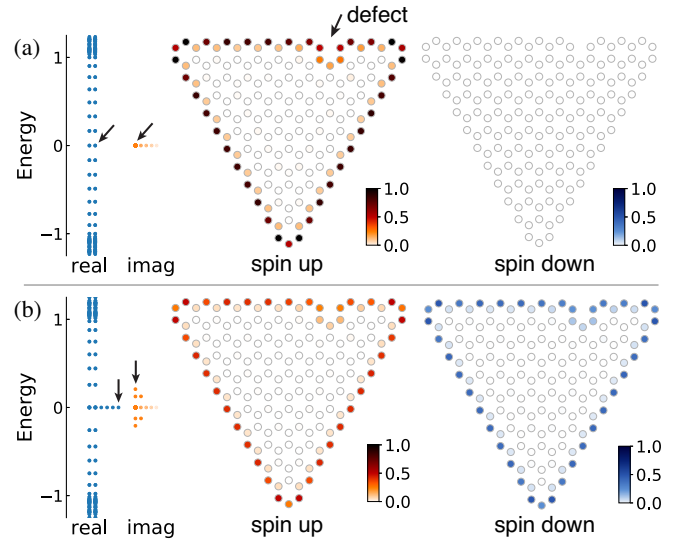

FIG. 3. Calculated wave functions of the model in Eq. (1) in a finite structure. (a) The eigenenergy spectrum without non-Hermitian couplings, and the wave function of the spin-up midgap edge state. The structure is a triangle with a defect on an edge. Degenerate energies in the spectrum are offset for visual clarity. The arrows mark the edge state that is plotted. The up-spin and down-spin components of the edge state are shown on the right. (b) The eigenenergy spectrum with non-Hermitian coupling and the wave function of the edge state with gain. Parameters used for this simulation: $t = 1$, $\lambda_{so} = 0.2$, $\gamma = 0.2 \times 3\sqrt{3}\lambda_{so}$.

can always enter the $\mathcal{PT}$-broken phase starting from the degenerate crossing point, in a region between two exceptional points, as is shown in Figs. 2(c) and 2(d). Thus, modal gain and loss only appear on the edge but not in the bulk, showing the topological edge-gain effect. Dynamics of the edge bands in the vicinity of the crossing point can be studied with an effective 2×2 Hamiltonian, and some details are given in the Supplemental Material [82].

In our model, the coupled edge states inherits the robustness against disorder from the edge states in a regular QSH system [4–7]. In the latter, a defect introduced on the edge will not cause reflection or localization as long as it does not flip the spins. This can be seen in Fig. 3a, where the edge state is extensively distributed in spite of a missing site on the edge. In our model, the non-Hermitian interaction induces a coupling between the spins. However, since the non-Hermitian coupling is uniformly distributed over the entire structure, the eigenstate consists of an admixture of the up and down spin eigenstates of a Hermitian QSH system. Consequently, the edge states of our non-Hermitian system carry over the robustness against order, as is observed in Fig. 3(b).

Such robustness against disorder has been exploited in the design of topological lasers, as it may help with suppressing the modal competition for better single-mode performance [12,49,50,52,70–79]. However, previous approaches to topological lasers are based on nonreciprocal models, which is challenging to implement in optoelectronic platforms. In contrast, our construction explores topological effects in a time-reversal invariant setting, which is compatible with standard photonic platforms such as photonic crystals or coupled ring resonator arrays. Moreover, with a uniform pumping everywhere in our

system, only the edge states have gain and thus can lase, while the entire bulk has zero gain. This is in contrast to previous works on topological lasers, where a spatially selective pumping scheme is usually required to ensure that only the edge state lases.

General recipe.—The topological edge-gain effect can be constructed in any QSH-like systems containing four bands or more, without the need of any additional symmetries such as time reversal or spatial inversion [82]. For a QSH system with time reversal and inversion symmetries, denoting $h_\uparrow(k)$ and $h_\downarrow(k)$ as the Hamiltonians of the two spins in the momentum space, the following form of a non-Hermitian Hamiltonian

$$H = \begin{pmatrix} h_\uparrow(k) & f_1(k)\kappa(k) \\ f_2(k)\kappa(k) & h_\downarrow(k) \end{pmatrix}, \quad \kappa(k) = h_\uparrow(k) - h_\downarrow(k), \quad (3)$$

provides the topological edge-gain effect, with arbitrary complex functions of $f_1(k)$ and $f_2(k)$, given that $f_1(k)f_2(k)$ is real. It can be shown that such a Hamiltonian satisfies pseudo-Hermiticity, which is considered as a generalization of $\mathcal{PT}$ symmetry [82,84–87]. With a non-Hermitian coupling strength that does not close the bulk gap, the bulk states remain without gain or loss, whereas the edge states always exhibit gain thorough a thresholdless phase transition. In our example model above, $\kappa = 2d_{15}(k)s^z$, and we have chosen $f_1(k) = f_2(k) = i\gamma/d_{15}(k)$.
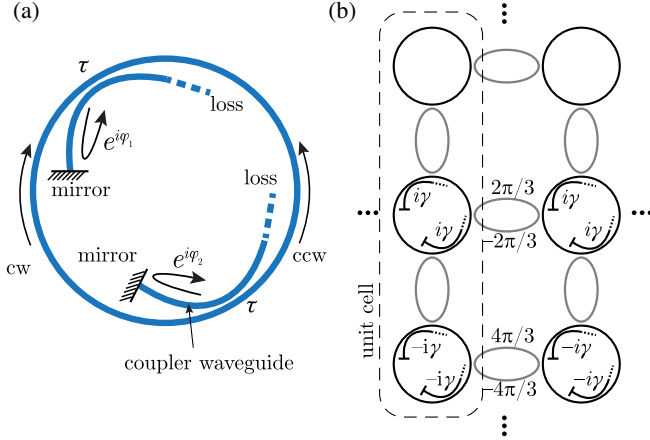
FIG. 4. Schematic of the coupled ring resonator arrays. (a) A ring resonator with two coupler waveguides inside. Each coupler waveguide has a lossy port on one end, and is reflecting on the other end. $1/\tau$ is the leakage rate into the couplers from the ring. $\phi_{1,2}$ are the phases accumulated by waves traveling from the coupling region to the mirror and back, which can be adjusted by changing the waveguide length. (b) A lattice of coupled ring resonator arrays creating a QSH system with effective magnetic flux of $1/3$. The lattice structure is identical to that of Ref. [16] except for the added waveguide couplers inside the ring resonators. The effective coupling induced by each coupler is marked aside the couplers. The effective phase of the linking rings for ccw waves are also marked on the linking rings.

Several well-known QSH models do have inversion symmetry, including the Kane-Mele model discussed above, the Bernevig-Hughes-Zhang model discussed in the Supplemental Material [6,7,82], and the model of magnetic flux on a lattice discussed in the following.

Implementation by coupled ring optical resonators.— Here we discuss an implementation of our model in coupled-ring optical resonator arrays. The structure is shown in Fig. 4, which is based on that studied in Refs. [16,49,70]. Here, the two spins are realized by the clockwise (cw) and counterclockwise (ccw) modes in each ring. To induce a non-Hermitian coupling between the two spins, we add two waveguide segments evanescently coupled to the ring resonator shown in Fig. 4(a) [88,89]. Each of the waveguides has a reflecting end and a lossy end. The cw (ccw) mode leak into the couplers, and in the designated coupler it gets reflected by the mirror and fed into ccw (cw), respectively. Each of such a ring is described by the following coupled-mode equation [82]:

$$i\frac{d}{dt}\begin{pmatrix} a_1 \\ a_2 \end{pmatrix} = \begin{pmatrix} -i\frac{2}{\tau} & i\frac{2}{\tau}e^{i\phi_1} \\ i\frac{2}{\tau}e^{i\phi_2} & -i\frac{2}{\tau} \end{pmatrix}\begin{pmatrix} a_1 \\ a_2 \end{pmatrix}, \quad (4)$$

where $a_{1,2}$ is the wave amplitude of the cw and ccw modes, respectively, $1/\tau$ is the leakage rate into the couplers, and $\phi_{1,2}$ are the phases accumulated by the wave traveling from the coupling region to the mirror and back. $\phi_{1,2}$ can be adjusted by tuning the lengths of the coupling waveguides.

The diagonal terms of $-2i/\tau$ in Eq. (4) are losses induced by the couplers, which can be compensated by a pumping of the gain medium in each ring resonator. The off-diagonal matrix elements in Eq. (4) give us the desired non-Hermitian couplings between the cw and ccw modes.

A lattice of coupled ring resonators with non-Hermitian couplings are shown in Fig. 4(b). Apart from the coupler waveguides in each ring, the structure is identical to that used in Ref. [16]. The Hamiltonian of this system takes the form

$$H = -t\sum_{x,y}(c^\dagger_{x+1,y}e^{-i2\pi\alpha y s^z}c_{x,y} + c^\dagger_{x,y+1}c_{x,y} + \text{H.c.})$$
$$+ \sum_{x,y}c^\dagger_{x,y}\begin{pmatrix} 0 & ie^{i\varphi}s_\mu\gamma^+_{|\mu|} \\ ie^{-i\varphi}s_\mu\gamma^-_{|\mu|} & 0 \end{pmatrix}c_{x,y}. \quad (5)$$

Here t is the hopping strength between nearest neighbor modes, $c_{x,y} = (c_{x,y,\uparrow}, c_{x,y,\downarrow})$ is the annihilation operator for the two spins on each site. The first line of the Hamiltonian describes a square lattice under a uniform magnetic field as described in the Landau gauge. $\alpha = p/q$ is the magnetic flux through each lattice unit cell, and p and q are incommensurate integers. The second line in Eq. (5) is the non-Hermitian coupling, constructed through the general recipe Eq. (3). Here, φ is an arbitrary phase, $\mu = \{[y + (q-1)/2] \bmod q\} - (q-1)/2$, s_μ is the sign of μ, $\gamma^\pm_0 = 0$, and $\{\gamma^{+,-}_{1,2,...,(q-1)/2}\}$ is a set of arbitrary real numbers.

We simulate the structure with a magnetic flux of $1/3$, and the photonic lattice is shown in Fig. 4(b). We adjust the in-ring couplers such that the non-Hermitian coupling coefficients for the three sublattice sites are 0, $i\gamma$, and $-i\gamma$, respectively. We calculate the band structure of this system in a stripe geometry that is periodic in x and finite in y with 300 cells. The results are plotted in Fig. 5. For this calculation, we assume $t = 1$ and $\gamma = 0.3$, whereas the threshold for the bulk $\mathcal{PT}$ phase transition is found numerically to be $\gamma \approx 0.7$. Again, although pumping is
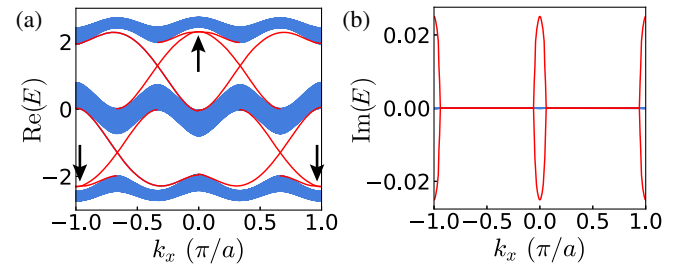

FIG. 5. Calculated band structure of the QSH system with non-Hermitian couplings in Fig. 4(b). The real and the imaginary parts of the eigenenergies are plotted in (a) and (b), respectively. The bulk bands are colored in blue, while the edge states in red. The location where edge states enter the $\mathcal{PT}$-broken phase is marked by the black arrows.

introduced throughout the ring-resonator arrays, gain only manifests on the edge but not in the bulk. Thus, same as the Kane-Mele QSH system discussed above, a topological localization of gain to the edge also occurs. The coupled ring-resonator array structure in Fig. 4(b) can be implemented through the same fabrication process as in previous experimental platforms [18,70].

In recent experimental studies of such a semiconductor ring-resonator setup, the reported topological gap was about 1 nm [49,67,70]. This leads to a 14 cm^{-1} modal gain differential between edge and the bulk [82]. Furthermore, the edge dominant mode with the highest gain becomes a lossless dark mode in the absence of pumping, whereas all other modes are lossy in this case. The fact that this edge mode is decoupled from the lossy ports guarantees the potential for low-threshold lasing.

In conclusion, we have shown that a uniform non-Hermitian topological material can have complex eigenvalues only in the edge states but not in the bulk. Such a topological edge-gain effect is protected by the bulk topology and $\mathcal{PT}$ symmetry, which lead to different $\mathcal{PT}$ phases in the bulk and on the edge. This effect can be generally induced in any topological material that contains two gapped subsystems, with a total of four bands or more. Such a separation of non-Hermitian phases between the bulk and the edge adds to the understanding of non-Hermitian topology. Our result provides the gain and loss control on the edge that is independent of the bulk, thus can be useful in various applications of non-Hermitian topological edge states. The designing of topological lasers can also benefit from this effect. In contrast to existing theoretical models for topological lasers, our construction is explicitly reciprocal. Furthermore, as gain is topologically localized to the edge, a nondegenerate lasing state is defined globally without the need of selective pumping.

Note added.—Recently, we became aware of a recent paper [90] that showed the topological gain effect in a specific system. The general condition to construct such an effect was not discussed in Ref. [90].

[*]shanhui@stanford.edu

[1] X.-L. Qi and S.-C. Zhang, Rev. Mod. Phys. **83**, 1057 (2011).

[2] M. Z. Hasan and C. L. Kane, Rev. Mod. Phys. **82**, 3045 (2010).

[3] J. Maciejko, T. L. Hughes, and S.-C. Zhang, Annu. Rev. Condens. Matter Phys. **2**, 31 (2011).

[4] C. L. Kane and E. J. Mele, Phys. Rev. Lett. **95**, 226801 (2005).

[5] C. L. Kane and E. J. Mele, Phys. Rev. Lett. **95**, 146802 (2005).

[6] B. A. Bernevig, T. L. Hughes, and S.-C. Zhang, Science **314**, 1757 (2006).

[7] M. Konig, S. Wiedmann, C. Brune, A. Roth, H. Buhmann, L. W. Molenkamp, X.-L. Qi, and S.-C. Zhang, Science **318**, 766 (2007).

[8] F. D. M. Haldane, Phys. Rev. Lett. **61**, 2015 (1988).

[9] D. J. Thouless, M. Kohmoto, M. P. Nightingale, and M. den Nijs, Phys. Rev. Lett. **49**, 405 (1982).

[10] Y. Hatsugai, Phys. Rev. Lett. **71**, 3697 (1993).

[11] A. B. Khanikaev and G. Shvets, Nat. Photonics **11**, 763 (2017).

[12] T. Ozawa, H. M. Price, A. Amo, N. Goldman, M. Hafezi, L. Lu, M. C. Rechtsman, D. Schuster, J. Simon, O. Zilberberg, and I. Carusotto, Rev. Mod. Phys. **91**, 015006 (2019).

[13] L. Lu, J. D. Joannopoulos, and M. Soljačić, Nat. Phys. **12**, 626 (2016).

[14] L. Lu, J. D. Joannopoulos, and M. Soljačić, Nat. Photonics **8**, 821 (2014).

[15] G. Q. Liang and Y. D. Chong, Phys. Rev. Lett. **110**, 203904 (2013).

[16] M. Hafezi, E. A. Demler, M. D. Lukin, and J. M. Taylor, Nat. Phys. **7**, 907 (2011).

[17] M. Hafezi, S. Mittal, J. Fan, A. Migdall, and J. M. Taylor, Nat. Photonics **7**, 1001 (2013).

[18] S. Mittal, S. Ganeshan, J. Fan, A. Vaezi, and M. Hafezi, Nat. Photonics **10**, 180 (2016).

[19] Y. Yang, Z. Gao, H. Xue, L. Zhang, M. He, Z. Yang, R. Singh, Y. Chong, B. Zhang, and H. Chen, Nature (London) **565**, 622 (2019).

[20] Q. Lin, X.-Q. Sun, M. Xiao, S.-C. Zhang, and S. Fan, Sci. Adv. **4**, eaat2774 (2018).

[21] A. V. Nalitov, G. Malpuech, H. Terças, and D. D. Solnyshkov, Phys. Rev. Lett. **114**, 026803 (2015).

[22] W. J. M. Kort-Kamp, Phys. Rev. Lett. **119**, 147401 (2017).

[23] M. C. Rechtsman, J. M. Zeuner, Y. Plotnik, Y. Lumer, D. Podolsky, F. Dreisow, S. Nolte, M. Segev, and A. Szameit, Nature (London) **496**, 196 (2013).

[24] A. B. Khanikaev, S. Hossein Mousavi, W.-K. Tse, M. Kargarian, A. H. MacDonald, and G. Shvets, Nat. Mater. **12**, 233 (2013).

[25] K. Y. Bliokh, D. Smirnova, and F. Nori, Science **348**, 1448 (2015).

[26] M. Onoda, S. Murakami, and N. Nagaosa, Phys. Rev. Lett. **93**, 083901 (2004).

[27] Z. Wang, Y. Chong, J. D. Joannopoulos, and M. Soljačić, Nature (London) **461**, 772 (2009).

[28] S. Barik, A. Karasahin, C. Flower, T. Cai, H. Miyake, W. DeGottardi, M. Hafezi, and E. Waks, Science **359**, 666 (2018).

[29] F. D. M. Haldane and S. Raghu, Phys. Rev. Lett. **100**, 013904 (2008).

[30] T. Liu, Y.-R. Zhang, Q. Ai, Z. Gong, K. Kawabata, M. Ueda, and F. Nori, Phys. Rev. Lett. **122**, 076801 (2019).

[31] K. Kawabata, K. Shiozaki, and M. Ueda, Phys. Rev. B 98, 165148 (2018).

[32] D. Leykam, K. Y. Bliokh, C. Huang, Y. D. Chong, and F. Nori, Phys. Rev. Lett. 118, 040401 (2017).

[33] J. M. Zeuner, M. C. Rechtsman, Y. Plotnik, Y. Lumer, S. Nolte, M. S. Rudner, M. Segev, and A. Szameit, Phys. Rev. Lett. 115, 040402 (2015).

[34] S. Weimann, M. Kremer, Y. Plotnik, Y. Lumer, S. Nolte, K. G. Makris, M. Segev, M. C. Rechtsman, and A. Szameit, Nat. Mater. 16, 433 (2017).

[35] S.-D. Liang and G.-Y. Huang, Phys. Rev. A 87, 012118 (2013).

[36] F. K. Kunst, E. Edvardsson, J. C. Budich, and E. J. Bergholtz, Phys. Rev. Lett. 121, 026808 (2018).

[37] H. Shen, B. Zhen, and L. Fu, Phys. Rev. Lett. 120, 146402 (2018).

[38] K. Esaki, M. Sato, K. Hasebe, and M. Kohmoto, Phys. Rev. B 84, 205128 (2011).

[39] S. Malzard, C. Poli, and H. Schomerus, Phys. Rev. Lett. 115, 200402 (2015).

[40] F. Dangel, M. Wagner, H. Cartarius, J. Main, and G. Wunner, Phys. Rev. A 98, 013628 (2018).

[41] J. Noh, W. A. Benalcazar, T. L. Hughes, and M. C. Rechtsman, in Conference on Lasers and Electro-Optics OSA Technical Digest (Optical Society of America, 2018), paper ID FM2Q.2.

[42] K. Kawabata, S. Higashikawa, Z. Gong, Y. Ashida, and M. Ueda, Nat. Commun. 10, 297 (2019).

[43] M. R. Hirsbrunner, T. M. Philip, and M. J. Gilbert Phys. Rev. B 100, 081104(R) (2019).

[44] M. Kremer, T. Biesenthal, L. J. Maczewsky, M. Heinrich, R. Thomale, and A. Szameit, Nat. Commun. 10, 435 (2019).

[45] Z. Gong, Y. Ashida, K. Kawabata, K. Takasan, S. Higashikawa, and M. Ueda, Phys. Rev. X 8, 031079 (2018).

[46] S. Yao and Z. Wang, Phys. Rev. Lett. 121, 086803 (2018).

[47] S. A. Hassani Gangaraj and F. Monticone, Phys. Rev. Lett. 121, 093901 (2018).

[48] C. Yuce, Phys. Rev. A 98, 012111 (2018).

[49] G. Harari, M. A. Bandres, Y. Lumer, M. C. Rechtsman, Y. D. Chong, M. Khajavikhan, D. N. Christodoulides, and M. Segev, Science 359, eaar4003 (2018).

[50] M. Seclì, M. Capone, and I. Carusotto, Phys. Rev. Research 1, 033148 (2019).

[51] K. Takata and M. Notomi, Phys. Rev. Lett. 121, 213902 (2018).

[52] B. Bahari, A. Ndao, F. Vallini, A. El Amili, Y. Fainman, and B. Kanté, Science 358, 636 (2017).

[53] X. Ni, D. Smirnova, A. Poddubny, D. Leykam, Y. Chong, and A. B. Khanikaev, Phys. Rev. B 98, 165129 (2018).

[54] J. Hou, Y.-J. Wu, and C. Zhang, arXiv:1910.14606.

[55] C. Yuce and Z. Oztas, Sci. Rep. 8, 17416 (2018).

[56] Y. C. Hu and T. L. Hughes, Phys. Rev. B 84, 153101 (2011).

[57] C. M. Bender and S. Boettcher, Phys. Rev. Lett. 80, 5243 (1998).

[58] Ş. K. Özdemir, S. Rotter, F. Nori, and L. Yang, Nat. Mater. 18, 783 (2019).

[59] Y. Li, Y.-G. Peng, L. Han, M.-A. Miri, W. Li, M. Xiao, X.-F. Zhu, J. Zhao, A. Alù, S. Fan, and C.-W. Qiu, Science 364, 170 (2019).

[60] J. Luo, J. Li, and Y. Lai, Phys. Rev. X 8, 031035 (2018).

[61] K. G. Makris, R. El-Ganainy, D. N. Christodoulides, and Z. H. Musslimani, Phys. Rev. Lett. 100, 103904 (2008).

[62] A. Guo, G. J. Salamo, D. Duchesne, R. Morandotti, M. Volatier-Ravat, V. Aimez, G. A. Siviloglou, and D. N. Christodoulides, Phys. Rev. Lett. 103, 093902 (2009).

[63] C. E. Rüter, K. G. Makris, R. El-Ganainy, D. N. Christodoulides, M. Segev, and D. Kip, Nat. Phys. 6, 192 (2010).

[64] Y. D. Chong, L. Ge, and A. D. Stone, Phys. Rev. Lett. 106, 093902 (2011).

[65] L. Feng, Y.-L. Xu, W. S. Fegadolli, M.-H. Lu, J. E. B. Oliveira, V. R. Almeida, Y.-F. Chen, and A. Scherer, Nat. Mater. 12, 108 (2013).

[66] L. Feng, Z. J. Wong, R.-M. Ma, Y. Wang, and X. Zhang, Science 346, 972 (2014).

[67] H. Hodaei, M.-A. Miri, M. Heinrich, D. N. Christodoulides, and M. Khajavikhan, Science 346, 975 (2014).

[68] A. Cerjan, A. Raman, and S. Fan, Phys. Rev. Lett. 116, 203902 (2016).

[69] L. Ge and A. D. Stone, Phys. Rev. X 4, 031011 (2014).

[70] M. A. Bandres, S. Wittek, G. Harari, M. Parto, J. Ren, M. Segev, D. N. Christodoulides, and M. Khajavikhan, Science 359, eaar4005 (2018).

[71] X.-C. Sun and X. Hu, arXiv:1906.02464.

[72] Y. V. Kartashov and D. V. Skryabin, Phys. Rev. Lett. 122, 083902 (2019).

[73] H. Zhao, P. Miao, M. H. Teimourpour, S. Malzard, R. El-Ganainy, H. Schomerus, and L. Feng, Nat. Commun. 9, 981 (2018).

[74] P. St-Jean, V. Goblot, E. Galopin, A. Lemaître, T. Ozawa, L. Le Gratiet, I. Sagnes, J. Bloch, and A. Amo, Nat. Photonics 11, 651 (2017).

[75] L. Pilozzi and C. Conti, Phys. Rev. B 93, 195317 (2016).

[76] R. Yao, H. Li, B. Zheng, S. An, J. Ding, C.-S. Lee, H. Zhang, and W. Guo, arXiv:1804.01587.

[77] S. Longhi, Ann. Phys. (Amsterdam) 530, 1800023 (2018).

[78] M. Parto, S. Wittek, H. Hodaei, G. Harari, M. A. Bandres, J. Ren, M. C. Rechtsman, M. Segev, D. N. Christodoulides, and M. Khajavikhan, Phys. Rev. Lett. 120, 113901 (2018).

[79] Y. Ota, R. Katsumi, K. Watanabe, S. Iwamoto, and Y. Arakawa, Commun. Phys. 1, 86 (2018).

[80] C. Yuce, Phys. Rev. A 97, 042118 (2018).

[81] H. Schomerus, Opt. Lett. 38, 1912 (2013).

[82] See Supplemental Material at http://link.aps.org/supplemental/10.1103/PhysRevLett.125.033603 for more information, which includes Ref. [83].

[83] H. A. Haus, in Waves and Fields in Optoelectronics (Prentice-Hall Inc., Englewood Cliffs, 1984), pp. 1–402.

[84] A. Mostafazadeh, J. Math. Phys. (N.Y.) 43, 3944 (2002).

[85] R. Zhang, H. Qin, and J. Xiao, J. Math. Phys. (N.Y.) 61, 012101 (2020).

[86] S. Nixon and J. Yang, Phys. Rev. A 93, 031802(R) (2016).

[87] P. Siegl, Pramana 73, 279 (2009).

[88] S. Fan, W. Suh, and J. D. Joannopoulos, J. Opt. Soc. Am. A 20, 569 (2003).

[89] Wonjoo Suh, Zheng Wang, and Shanhui Fan, IEEE J. Quantum Electron. 40, 1511 (2004).

[90] K. Kawabata, K. Shiozaki, M. Ueda, and M. Sato, Phys. Rev. X 9, 041015 (2019).